



HAL
open science

Balloon-borne measurement of the aerosol size distribution from an Icelandic flood basalt eruption

Damien Vignelles, T. Roberts, E. Carboni, E. Ilyinskaya, M. Pfeffer, P. Dagsson Waldhauserova, A. Schmidt, Gwenaël Berthet, Fabrice Jegou, Jean-Baptiste Renard, et al.

► To cite this version:

Damien Vignelles, T. Roberts, E. Carboni, E. Ilyinskaya, M. Pfeffer, et al.. Balloon-borne measurement of the aerosol size distribution from an Icelandic flood basalt eruption. *Earth and Planetary Science Letters*, 2016, 453, pp.252 - 259. 10.1016/j.epsl.2016.08.027 . insu-01382430

HAL Id: insu-01382430

<https://insu.hal.science/insu-01382430>

Submitted on 17 Mar 2020

HAL is a multi-disciplinary open access archive for the deposit and dissemination of scientific research documents, whether they are published or not. The documents may come from teaching and research institutions in France or abroad, or from public or private research centers.

L'archive ouverte pluridisciplinaire **HAL**, est destinée au dépôt et à la diffusion de documents scientifiques de niveau recherche, publiés ou non, émanant des établissements d'enseignement et de recherche français ou étrangers, des laboratoires publics ou privés.

Balloon-borne measurement of the aerosol size distribution from an Icelandic flood basalt eruption

D. Vignelles¹, T.J. Roberts¹, E. Carboni², E. Ilyinskaya³, P. Dagsson Waldhauserová⁴, M. Pfeffer⁵, G. Berthet¹, F. Jegou¹, J.-B. Renard¹, H. Olafsson⁶, B. Bergsson⁵, R. Yeo⁵, N. Fannar Reynisson⁵, R.G. Grainger², B. Galle⁷, V.C. Jacobo⁷, S. Arellano⁷, T. Lurton¹, B. Coute¹ and Vincent Duverger¹

¹ LPC2E/CNRS / Université d'Orléans, 3A, Avenue de la Recherche Scientifique 45071 Orléans, France

² COMET, Atmospheric, Oceanic and Planetary Physics, University of Oxford, Parks Road, Oxford, OX1 3PU, U.K.

³ British Geological Survey, Murchison House, West mains road, Edinburgh EH9 3LA, United Kingdom

⁴ Agricultural University of Iceland, Faculty of Environmental Sciences, Hvanneyri, Iceland

⁵ Icelandic Meteorological Office, Bústaðavegi 7-9, 150 Reykjavik, Iceland

⁶ University of Iceland, Icelandic Meteorological Office and Institute for Meteorological Research, Reykjavík, Iceland

⁷ Chalmers University of Technology, Department of Earth and Space Sciences, Hörsalsvägen 11, 412 96 Gothenburg, Sweden

Abstract.

In situ balloon borne flight measurements of the aerosols emitted by the Icelandic volcano Holuhraun plume have been realized on January 22nd 2015 at 21UTC. We present several data sets that we recorded during the balloon flight which intercepted the plume at 8km distance downwind from the crater, which represents a “young” plume age of approximately 15 minutes. We show in particular the aerosol size distribution measured by a novel miniature optical particle counter called LOAC (Light Optical Aerosol Counter) which determines both the number and size distribution of particles, alongside a meteorological payload. Compared with both local and distant independent SO₂ measurements, we discuss calculated aerosols flux emitted by Icelandic volcano.

The balloon passed through a plume located between 2 and 3.1 km in altitude above sea level. Two plume layers were observed, a non-condensed lower layer and a condensed upper layer. The lower layer of 400m thick was characterized by a modus of fine particles centered on 0.2 μ m in diameter and a second modus centered on 2.3 μ m in diameter and a total particle concentration

35 around 100 particles per cubic centimeter. The upper layer of 800m thick was a cloud-like signature
36 with droplets centered on 20 μm in diameter and a fine modus, the measured total particle
37 concentration was 10 times higher than the first layer. The plume top height was determined
38 between 2.7 and 3.1 km, the plume height is in good agreement with an estimate made by analysis
39 of IASI satellite remote sensing data.

40 This experimentation shows that under such difficult field campaign conditions (strong wind, low
41 temperatures, only car batteries for power supply, night time and active volcano close to the launch
42 site) it is possible to launch meteorological balloons with novel payloads to directly sample in-situ the
43 near-source plume, determine the plume altitude, identify dynamical phases of the plume and
44 document the size distribution of particles inside a plume which is only a quarter of an hour old.

45 **1. Introduction**

46 Volcanoes release gases and particles to the atmosphere through continuous degassing, or
47 episodic eruption events, and depending on the injection altitude they can impact both tropospheric
48 and stratospheric composition and climate. Ash-rich emissions such as the Icelandic Eyjafjallajökull
49 eruption in 2010 can lead to widespread disruption of aviation (Spinetti et al., 2013). Ash-poor
50 volcanic plumes can also strongly impact the environment and quality of life due to high
51 concentrations of polluting gases and aerosol particles. Indeed, the recent 'Flood basalt' fissure
52 eruption at Holuhraun (31 August 2014 – 27 February 2015, 1,6km³ of eruptive lava, Gislason et al.
53 2015) was a major source of sulfur gases and aerosols and caused both local (Gislason et al. 2015)
54 and European-wide (Schmidt et al. 2015) deteriorations to air quality.

55 Flood basalt eruptions are one of the most hazardous volcanic scenarios in Iceland and had
56 enormous societal and economic consequences across the northern hemisphere. One of the best
57 known examples is the Laki eruption (1783-84 CE) (Thordarson and Self, 2003) which caused the
58 deaths of >20% of the Icelandic population by environmental pollution and famine (Thordarson and
59 Self, 2003) and likely increased European levels of mortality through air pollution by sulfur-bearing
60 gas and aerosol (Witham and Oppenheimer, 2004). Potential impacts of such an eruption on modern
61 day Europe have been modelled by Schmidt et al. (2011) who found that PM_{2.5} aerosol pollution
62 would double in concentration causing 142,000 (8-9%) additional cardiopulmonary fatalities in the
63 year following eruption onset. A Laki-type eruption scenario has been recently included in the UK
64 National Risk Register. However, there are still many uncertainties about the source terms of
65 Icelandic flood basalt eruptions which are necessary for atmospheric models and health impact
66 assessments. Holuhraun eruption was therefore a unique opportunity to study at first hand the near-
67 source composition of a volcanic plume from an Icelandic flood basalt.

68 The capability of atmospheric models to predict volcanic plume impacts is limited by uncertainties
69 in the near-source plume state. Most in-situ measurements of the elevated plume involve
70 interception of more aged plumes that have already chemically or physically evolved. Small portable
71 sensors airborne drone or balloon platforms offer a new possibility to characterize volcano plumes
72 near to source. McGonigle et al. (2008) has demonstrated heli-type drone sensing of SO₂ and CO₂ to
73 determine CO₂ fluxes at Volcano fumarole field. Recently, Shinohara (2013) deployed a suite of gas
74 sensors on a drone to characterize the plume of Shinmoedake, Kirishima volcano, Japan during a
75 hazardous eruptive phase that prevented ground-based sampling. Pieri et al. (2013) performed drone
76 as well as balloon-based campaigns to measure gases and ash in the eruption plume of Turrialba
77 volcano in Costa Rica. Measurements of volcanic aerosol (non-silicate particles, such as sulfate) are
78 also needed to better constrain the plume sulfur chemistry and particle processes, which together
79 with plume injection height are two key uncertainties in models used to predict the dispersion and

80 air-quality impacts from eruptions. Here we deployed a newly developed lightweight optical aerosol
81 counter (LOAC) on a meteorological balloon through the Holuhraun eruption plume at source.
82 Through measurements of size-resolved volcanic aerosol together with meteorological parameters
83 we are able to provide key eruption source term information.

84 **2. Methods**

85 **2.1 Balloon Instrumentation**

86 The LOAC (Light Optical Aerosol Counter) is an optical particle counter sufficiently light-weight to
87 be carried by a 1000gr meteorological balloon. The instrument contains a laser (650nm) and
88 measures the intensity of light scattered at two angles, 12° and 60°, (Lurton et al., 2014; Renard et
89 al., 2015) to discriminate the particle concentration over 19 size classes from 0.2 to 100µm in
90 diameter. Sampling is made with a miniature pump (2 L/min) enclosed in the gondola, the air
91 sampled is released after passing through the measurement cell. For the LOAC integration time of
92 10s, the counting uncertainty is derived from the Poisson counting statistics and defined as the
93 relative standard deviation: 60% for aerosol concentration of 10^{-2} cm^{-3} , 20% for 10^{-1} cm^{-3} and 6% for
94 concentrations higher than 1 cm^{-3} . A complete description of the instrument can be found in Renard
95 et al. (2015). Differences in scattering between two distinct angles are also used to characterize the
96 main nature of the aerosols (carbonaceous particles, sand, liquid droplets, salt), with reference to
97 laboratory calibration samples, referred to as typology. As well as aerosol data, GPS coordinates,
98 temperature and hygrometry are recorded in real time thanks to a telemetry system.

99 To aid interpretation, the balloon data are analyzed in conjunction with model outputs
100 (trajectory, air quality plume dispersion and meteorological models) and remote sensing data
101 (ground-based DOAS, and satellite IASI overpasses) as discussed in the Results.

102 **3. Results**

103 **3.1 Holuhraun plume conditions**

104 On January 22nd 2015, day of the balloon release, visible plumes were emitted from several
105 different locations from the crater and lava field (figure1). The largest part of the emitted gas
106 volume (about 90%) was released from the main vent named Baugur, where fresh magma was being
107 erupted. The remaining gas emissions were sourced from the active lava flows traveling away from
108 Baugur. These different plumes merged into one main plume that was advected northeastward.
109 While it rose in altitude, the thermally buoyant plume visibly changed dynamical conditions, with the
110 upper part of it turning into (an optically thick) cloud at several kilometers downwind from the
111 source. The atmosphere was very clear within the boundary layer, and the lower troposphere was
112 observed to be cloud-free except for the volcano plume cloud. Clouds were visible at much higher
113 altitude (over 5.5 km as described in section 3.3.1). Figure 1 illustrates the Holuhraun plume as it was
114 on January 22th at 14UTC. From the morning until the end of daylight, the plume exhibited visually
115 very consistent behavior as described above. Atmospheric modelling (Iceland Met Office, CallPuff
116 model, Barsotti et al. 2008.) predicted that the northeastward plume advection continued during the
117 night, when our balloon-based measurements were performed (figure 2). Although this modelling
118 output reflects the ground plume exposure, the constant vertical wind profile of the HARMONIE
119 model in the Holuhraun zone (see discussion in section 3.3) justifies us to assume locally a similar
120 plume dispersion from the ground up to 4 km altitude, as a guide to our balloon launching
121 experiment.

122 **3.2 Balloon flight**

123 The meteorological balloon and measurement instrumentation were prepared during the evening
124 of January 22nd, on site. The balloon was inflated during the night time, with a ground air
125 temperature below 0° Celsius and relatively high wind speed of about 10m/s. The ground telemetry
126 station was powered only by car batteries at this remote launch site. This situation was a
127 combination of such difficult conditions for this kind of operation that making this balloon profile of
128 the near-source plume represented a considerable challenge.

129 The balloon borne instruments were launched at 64°56'01"N & -16°40'39"E at 21 UTC on January
130 22nd 2015, 9 kilometers N-NE from the Holuhraun main eruptive crater (64°52'21"N & -16°49'42"E),
131 and at around 700m above sea level. This launch site (directly under the plume) was chosen based on
132 visual observations of plume advection made before night time, and output from the the HARMONIE
133 model (figure 2). At this distance from the crater and given the dispersion of the plume, we were
134 assured that a balloon launched from this location would cross the plume. Backward trajectories over
135 the launching site confirm that the air mass movement was in the right direction, arriving from
136 Holuhraun eruptive crater (figure 3). The backward trajectories are calculated with FLEXTRA 5.0 code
137 which is a 3D kinetic trajectory calculation code (Stohl et al. 1999). Trajectories are initialized using
138 global 3-hourly ECMWF reanalysis data with 1°x1° horizontal resolution for a period of 24h hours
139 from 21 UTC on January 22nd and at every 200m above the balloon launching position up to 14 km.
140 For clarity, Figure 3 presents only the backward trajectories initialized at 2400m and 4000m,
141 corresponding to the height of the plume and the air mass above the plume respectively. It must be
142 noted that all trajectories showed the same direction of advection indicating that the wind direction
143 was similar between the ground to altitudes higher than the top of the plume (as determined by
144 aerosol observations, see section 3.3). Based on the FLEXTRA backward trajectories, we were also
145 able to determine the average age of the plume when the balloon crossed it, considering only a
146 horizontal advection and constant velocity of the air mass between the two final hours of the
147 trajectories. This calculation gives an air mass age between 10 and 15 minutes.

148 Physical parameters were recorded during the ascent and transmitted by telemetry. The
149 meteorological parameters were recorded with a frequency of 1Hz whereas the particles
150 concentration measured by the LOAC aerosol counter is given for each size class every 10 seconds
151 and the typology relative to the optical properties of aerosols is provided every 60 seconds. The
152 typology is a specific term relative to the index of optical particles refraction properties obtained by
153 combining the intensities of light scattered at two specific angles (Renard et al., 2015). It can provide
154 information on the nature of the particles, determined by reference to laboratory measurements
155 (Renard et al., 2015). The typology gives several classes of optical properties discussed in section 3.4.
156 Due to a technical problem with the data telemetry system, the concentration data was not recorded
157 from the ground to around 1700m. Data were recorded from 1700m above the sea level (asl) to
158 8000m asl with a small number of data points lost during telemetry, mostly in the altitude range
159 between 4.4 and 4.8 km asl.

160 **3.3 Determination of zones**

161 Figure 4 shows the vertical velocity of the balloon, the relative humidity (RH) and the total
162 concentration of particles (TPC) between 0.2 and 100 µm in diameter as a function of altitude. On
163 each plot we have determined 6 zones to discriminate several structures. These zones are
164 represented by grey surfaces and numerated from the bottom on figure 4. These 6 distinct zones
165 were determined based on correlations found between RH and aerosol profile. Figure 5 presents the
166 observed aerosol size distribution as a function of altitude. For the size-dependent particle
167 concentration, the number in each size class is represented by a color relative to the color scale on
168 the left, the concentration is normalized by the range of size classes and is expressed as $dn/d\log(d)$

169 where n is the concentration and d the mean diameter of the class size. On the right panel, we show
170 the optical typology detected by the LOAC for six groups of size classes. Each color represents the
171 bulk nature of the aerosol shown by the color scale on the right of the graph. Most notable are two
172 distinct zones of liquid droplets (around ~2.5-3 km altitude) and ice particles (around ~6-7 km
173 altitude, zone 6) which correspond to distinct water/ice cloud layers. Further discussions of the
174 aerosol size distribution and its typology across the identified zones are given in Section 4.

175 Zone 1 determined from 1.7 to 2.0km above sea level, presents a high and structured vertical
176 balloon velocity profile, an increasing RH with altitude and a relatively low concentration of particles
177 (around 5 particles per cm^{-3} over the 0.20 μm to 100 μm detection range). This zone is representative
178 of the atmosphere near from the ground and under the plume.

179 Zone 2 from 2.0 to 2.3km above sea level, is characterized by a higher RH and higher particle
180 concentration than the zone 1 (around 100 particles per cm^{-3}). The particle size distribution,
181 discussed below, shows a second mode and the typology indicates a distinct mean nature of particles
182 corresponding to absorbing particles. The zone 2 is the plume in a non-condensed phase.

183 Zone 3 is the plume in the condensed phase determined between 2.3 and 3.1 km above the sea
184 level. The particle concentration is above 500 particles per cm^{-3} , and the typology indicates liquid
185 droplets. This assumption is validated by the rapidly decreasing vertical velocity measured above 2.3
186 km which indicates a change in the air mass composition: above this altitude some liquid droplets
187 condensed onto the balloon, increasing the mass of the balloon which caused the vertical velocity to
188 decrease from 10 to 4 $\text{m}\cdot\text{s}^{-1}$. This deduction is consistent with the hygrometry measurements which
189 indicate a high RH above 2.3 km. The section 3.4 discusses the distribution in size measured in the
190 zone 3 and shows clearly that the aerosols are composed by droplets. We determined the upper part
191 of the zone 3 at 3.1 km even if the concentration of particles in 2.8 to 3.0 km band is close to the
192 background level. We assume dynamical processes can locally modulate the aerosol concentration
193 profile (plume layering). Here, the top of the plume is assumed to be between 2.8 and 3.1 km, which
194 represents a very precise localization and is in good agreement with an estimate from satellite data
195 as discussed further in section 3.3.2. In order to determine if zone 3 is a condensed plume or an
196 atmospheric cloud above the eruptive location, we have used a non-hydrostatic convection-
197 permitting model developed by Météo-France and ALADIN based on the AROME model from Météo-
198 France (Seity et al, 2011, Brousseau et al. 2011) named HARMONIE. Firstly, outputs from the
199 HARMONIE model for both 14UTC and 22UTC focused on the Holuhraun region confirms that the
200 meteorological situation was very similar during the daytime when the photograph was taken (Figure
201 1) and nighttime when we launched the balloon, i.e. that there were no atmospheric clouds at this
202 altitude. Figure 6 presents the temperature and the dew point for both day and night cases, showing
203 very similar profiles in temperature, maximum dew point and wind direction at 14UTC and 22UTC.
204 Secondly, the output from HARMONIE does not clearly indicate any low-level cloud. This model is not
205 sensitive to the events such as Holuhraun eruption and therefore presents the meteorological
206 conditions without the contribution of the volcanic plume. This result further confirms that the high
207 aerosol and cloud droplets that we have visually observed at 14UTC and measured at 22UTC is
208 actually the plume in a condensed phase visible on figure 1.

209 Zone 4 is the overlying air mass without the influence of the plume. A low total aerosol
210 concentration was found in this zone, around 5 to 10 particles per cm^{-3} over the 0.20 μm to 100 μm
211 detection range. This zone represents the background conditions and was found to be constant as a
212 function of altitude even though the RH measurements still exhibit high values between 3.1 and 3.6
213 km which may be an instrument effect caused by persistence of humidity on the sensor. The

214 concentration and size distribution in this zone 4 is similar to the signature found in zone 1, thus the
215 boundaries between zone 1-2 and 3-4 and determine the bottom and the top level of the plume.

216 Zone 5 and 6 are discussed here only briefly in order to show the complete profile of flight.
217 Between 4.4 and 4.9km we lost the signal from the gondola. Zone 5 is assumed to be a background
218 air mass influenced by the icy cloud determined by zone 6. The typology clearly identifies the
219 particles to be icy cloud in zone 6 corresponding to the high altitude clouds visible on figure 1.

220 4. Discussion

221 4.1. Plume Height

222 Our balloon-based measurement of plume height (2 and 3.1km, with condensed phase layer
223 between 2.3km and 3.1km) is a key constraint needed for models of the downwind plume dispersion.
224 We compare our plume height observation to an independent estimate of the plume height as well
225 as the SO₂ column analysis from IASI data on METOP Satellite. This novel technique to retrieve plume
226 height from satellite data is described by Carboni et al. (2012) and has been applied to several
227 volcanic eruptions in Carboni et al. (2015). Here we only report a summary of the algorithm. The
228 optimal estimation technique of Rodgers (2000) is employed to estimate SO₂ plume, and the surface
229 skin temperature using simultaneously all IASI measurements from 1000 to 1200 cm⁻¹ and from 1300
230 and 1410 cm⁻¹ (the ν_1 and the ν_3 SO₂ bands). The retrieval is effected by minimizing a cost function J
231 defined as

$$232 \quad J = (\mathbf{y} - \mathbf{F}(\mathbf{x})) \mathbf{S}_y^{-1} (\mathbf{y} - \mathbf{F}(\mathbf{x}))^{-1} + (\mathbf{x} - \mathbf{x}_a) \mathbf{S}_a^{-1} (\mathbf{x} - \mathbf{x}_a)^{-1}$$

233 Where $\mathbf{F}(\mathbf{x})$ is the forward model (i.e. the function which maps the state parameters to
234 measurements), \mathbf{x} is the vector of retrieved values, \mathbf{y} the measurement vector, \mathbf{S}_y is the
235 measurement error covariance matrix, \mathbf{x}_a is the a priori error covariance matrix. The forward model is
236 based on RTTOV (Saunders et al. 1999) extended to include SO₂ explicitly, and uses ECMWF
237 temperatures interpolated to the measurement time and location. Note that the SO₂ IASI retrieval is
238 not affected by underlying cloud and rigorous error propagation, including the incorporation of
239 forward model and forward model parameter error, is built into the system, providing quality control
240 and error estimates on the retrieved state for every pixel. Figure 7 shows the contribution of three
241 overpasses of METOP over Iceland on January 22nd at 18, 19 and 20 UTC (within hours of our balloon
242 flight). Each measurement is represented by a symbol and a color. Symbols are relative to the hour
243 where the satellite overpassed (a star for 18 UTC, a cross for 19 UTC, a diamond for 20 UTC). Colors
244 represent the retrieved plume altitude. The altitude given by the Carboni algorithm of the closest
245 measurement from the crater is 3.0 ± 1.1 km. This altitude is consistent with the altitude detected by
246 the LOAC which determines the top height of plume in the 2.7-3.1 km range, although the two
247 estimates are based on data collected 30 kilometers apart. Thus the LOAC balloon flight contributes
248 to the in-situ validation of the recently developed Carboni et al. (2012, 2015) method for the plume
249 altitude estimation by IASI satellite retrieval. Altitude estimation of volcanic plumes is critical both for
250 modelling plume advection, chemical processing and atmospheric impacts, and can be a key
251 uncertainty in the estimation of SO₂ burdens from satellite.

252 4.2. Particle size distribution in the plume

253 In this section we investigate the size-distribution in the different altitude zones in detail. Figure 8
254 presents the particle size distribution in zones 1 to 4. The left panel shows the size distribution in
255 each zone averaged across the number of points that were recorded by telemetry during the ascent
256 and presented in dn/dLog(d). Every 10 seconds the LOAC measures a distribution in size over 19 size

257 classes from 0.2 to 100 μm , these data are presented in the left panel with thin grey lines and the
 258 mean average shown with thick black line with diamonds. On the right, for each average size
 259 distribution we have calculated the volume distribution assuming spherical particles with diameter
 260 centered on the mean diameter of the size class. For each volume distribution we fitted log normal
 261 distribution modes described by equation (1), also shown in the right panel of Figure 8 table 1.

$$262 \quad V(d) = \frac{V_0}{\sigma_N \sqrt{2\pi}} e^{\left(-\frac{1}{2} \left(\frac{\log(d) - \mu_V}{\sigma_N} \right)^2 \right)} \quad (1)$$

263 Where $V(d)$ is the volume density distribution with shape parameters: σ_N and μ_V and the amplitude
 264 parameter V_0 were determined by least-squares fitting to the LOAC observations.

265 Firstly, we observe that the size and volume distributions for zones 1 and 4 (both identified as
 266 background air, outside of plume) are of similar proportions, with similar mean diameter and
 267 standard deviation. The difference in total number of particles between the zone 1 and 4, higher in
 268 smallest size for the zone 1 closer to the ground, is likely due to wind erosion and different aeolian
 269 processes. Holuhraun is located northward from the largest Icelandic Glacier Vatnajökull in the
 270 largest desert area of Iceland called Dyngjúsandur (Arnalds, 2010; Baratoux et al., 2011; Dagsson-
 271 Waldhauserova et al., 2013, 2014). Dyngjúsandur consists of sand dominated by glass grains from
 272 several volcanic eruptions of Askja, Bardabunga and Kverfjöll in the past (Baratoux et al., 2011;
 273 Oladottir et al., 2011), while a mixture of volcanic materials was likely added also during the
 274 Eyjafjallajökull 2010, Grímsvötn 2011 and Holuhraun 2014-2015 eruptions. Dyngjúsandur dust is
 275 frequently suspended during storms (Dagsson-Waldhauserova et al., 2013). These dust events
 276 occurred, however, mostly during the summer-autumn period, whilst resuspension of snow may be a
 277 wind-driven surface source of particles in winter. We assume that this mono-modal background
 278 particle distribution is also a representative background for zones 2 and 3 where plume was present.
 279 Clear bimodal particle distributions are observed in these zones 2 and 3, which dominate over the
 280 background signature. The bimodal distribution consists of sub-micron and supra-micron modes in
 281 zone 2, attributed to non-condensed plume. In the condensed plume of zone 3 these modes have
 282 greater diameter.

283 More precisely, zone 2 presents a size distribution that is higher in number than the zone 1 for
 284 particles smaller than $1\mu\text{m}$, with the first mode maximum below detection range ($< 0.2\mu\text{m}$), and with
 285 a second mode around $2\mu\text{m}$ (all parameters are summarized in Table 1). This observation is strikingly
 286 similar to ground-based observations of volcanic aerosols in the plume of quiescently degassing Mt
 287 Etna, made using a hand-held LOAC instrument at $\sim 1\text{ km}$ downwind from the volcano summit
 288 (Roberts et al., 2015), a similarly bi-modal distribution was found, with similar sub-micron and supra-
 289 micron modes. Interestingly, our Holuhraun measurements made 8 km from the source observe a
 290 greater proportion of particle volume in the smaller mode relative to the larger mode than for the
 291 Etna measurements made just $\sim 1\text{ km}$ from the source. This difference might reflect a greater extent
 292 of near-downwind plume processing during the 15 min (8 km) plume transport but might also reflect
 293 differences in the nature of these two volcanic emission sources (which vary in both emissions,
 294 strength and composition). Further observations of a range of volcanic plumes under different
 295 conditions are needed to distinguish these two possible explanations.

296

297 The zone 3 condensed plume exhibits a first mode at somewhat greater diameter than in zone 2,
 298 and a second mode with diameter $19\mu\text{m}$. Such particle modes around $10\mu\text{m}$ are characteristic of
 299 clouds (Warner 1969, Hammer et al. 2014). Typology clearly shows the existence of liquid droplets.

300 Water cloud droplet formation is expected given presence of submicron particles even in the
301 background air as well as the plume that can act as cloud condensation nuclei also noting the
302 Holuhraun eruption produced very little ash. The measured vertical concentration profile in the zone
303 3 might be affected by an instrumental effect called the shadowing effect that lead to underestimate
304 the number of fine particles when larger particles are simultaneously detected (due to a scattering
305 coincidence effect in the measurement cell see Renard et al. 2015, and Roberts et al., 2015 who
306 identified this effect under strong volcanic plume conditions). In addition, a reduced number of small
307 particles in the presence of larger particles might indicate the process of fine particles growing into
308 larger particles leading to a transfer from the smallest size to larger. The phenomenon is significant
309 between 2.4km and 2.7km where large particles in the first layer of condensed plume appear, see
310 Figure 4, 5. This part of zone 3 is flanked by two peaks with fewer large particles and greater than 10
311 times the concentration of smaller particles than the inner region where a greater number of large
312 particles are detected. It is also indicative of plume heterogeneity.

313 Above the plume in zone 4, the particle size distribution is relatively constant and close to the
314 distribution in size measured in zone 1 (with typology shows high complex refractive index relative to
315 absorbing particles), until the icy cloud becomes present between 5.5 and 7 km (zone 5). This occurs
316 in a region of higher RH and is highlighted both by both the size-resolved aerosol number and the
317 speciation index, Figure 5.

318 **4.3. Optical particles index, the “Typology”**

319 For zone 2, the speciation index relative to the optical properties of particles does not reveal a
320 clear optical nature of particles. It gives optically absorbing signature, however we believe the
321 observed particles to be most likely dominated by sulfate, based on particle measurements from
322 non-explosive ash-poor volcanic emissions made elsewhere (e.g. Kroll et al., 2015). Volcano
323 emissions are chemically reactive and the sulfate aerosol can be formed through high-temperature
324 near-vent chemistry as well as low-temperature atmospheric oxidation of emitted SO₂ (e.g. Roberts
325 et al., 2014). A possible complexity to determining speciation from particle scattering can be the
326 presence of internally mixed aerosol, or particles of different kinds in the same sampling period.
327 Volcanic aerosol can be a complex mixture, with sulfate typically as a major component but also
328 containing e.g. metal salts. Roberts et al. (2015) determined that the LOAC measurements of aerosol
329 in Etna grounding plume were fully consistent with having a predominantly aqueous sulfate
330 composition (as determined from volume calculations with co-measured SO₂), but also observed an
331 absorbing signature in the LOAC typology, proposed to be caused by additional contaminants within
332 the sulfate aerosol which can have a disproportionate effect on the overall typology. However, no
333 further conclusion on the precise Holuhraun particle composition can be made here. Nevertheless,
334 the result is that the nature of the particles are distinct between zones 1 and 2. Certainly the plume
335 did not contain substantial quantities of volcanic ash. This is confirmed by the quiescent nature of
336 the degassing (in stark contrast to the explosive Icelandic Eyjafjallajökull eruption of 2010 see
337 Spinetti et al. 2013) and in-field visual observations made during the eruption. The reddish-brown
338 hue of the plume in Figure 1 is most likely attributed to an optical effect of back-scattered sunlight
339 from the aerosols.

340 In zone 3 the typology gives an unambiguous droplets signature. Here the condensed phase is
341 clearly established. This also confirms the hygroscopic nature of the volcanic particles. Condensed
342 water on the volcanic particles both increases their size (section 3.3) and acts to dilute any absorbing
343 component to the extent that the typology yields a droplets signature.

344 The typology is less well resolved over the altitude profile than the concentration but also
345 indicates the same plume layering: in the 2.8-3.0 altitude range where a thin layer of non-condensed
346 plume was found (section 3.3).

347 Typology is similar for the zone 4 and zone 5. Typology for zone 6 is also very well established as
348 being distinct to the previous zones and indicates ice. The presence of icy clouds at high altitudes is
349 thus clear.

350 **4.4. Particle flux**

351 Over the 1 km thick non-condensed part of the plume (zone 2) the LOAC instrument measured on
352 average about 100 particles per cm^{-3} over the class size range 0.2 to $100\mu\text{m}$ in diameter. Using this
353 particle concentration observation we attempt a calculation to coarsely estimate the particle
354 emission from Holuhraun. This cannot be calculated directly from the aerosol and plume depth
355 observations because the width of the plume is unconstrained. Neither was SO_2 co-measured during
356 the LOAC balloon flight, therefore the calculation is only approximate. We calculate a ratio number of
357 particles per kg of SO_2 by comparing the balloon-based aerosol observations to remote sensing SO_2
358 observations by DOAS scanning the plume 10 km from the crater and from IASI satellite, and
359 combine with the total flux of SO_2 released in January 2015 to finally estimate the number of
360 particles emitted on the whole period.

361 The NOVAC scanning DOAS (Galle et al. 2010) is positioned 10 km eastward from the Baugur vent
362 ($64^\circ53'3.78''\text{N}$; $16^\circ40'31.70''\text{O}$). The scanning NOVAC DOAS instrument uses scattered sunlight in the
363 UV region to derive path-integrated concentrations (columns) of SO_2 . The instrument's viewing
364 direction is rotated along a conical surface from horizon to horizon. When this cone intersects a
365 plume, the total number of molecules of SO_2 in a cross section of the plume can be determined, and
366 the flux through the cross section was calculated with the NOVACProgram software using wind
367 speeds and directions determined by the HARMONIE numerical prediction model and a plume height
368 of 1387 m, which is the average triangulated plume height when two DOAS instruments detected the
369 plume. Column SO_2 density of up to 800 DU (time average of 200 DU) was detected on the day of the
370 flight (one Dobson unit (DU), is equivalent to 2.69×10^{16} molec. cm^{-2} SO_2 column). An average
371 emission rate of 400 kg/s SO_2 for this day was calculated using wind parameters provided by the
372 HARMONIE numerical prediction model. Assuming 200 DU SO_2 , 100 particles per cm^{-3} and plume of
373 1km thick, a ratio of 1.75×10^{13} particles per kg of SO_2 is calculated. Combining with the 400 kg/s SO_2
374 flux yields a coarsely estimated flux of 6×10^{20} volcanic particles in the range of 0.2 and $100 \mu\text{m}$
375 emitted by Baugur vent during this day. The same estimation with IASI data at 2 DU SO_2 (figure 7)
376 gives 10^{15} particles per kg of SO_2 and 6×10^{22} particles emitted during this day. Two magnitudes of
377 difference on these estimations can be due to the difference in the field of view of the methods and
378 the non-collocation of measurements. The IASI data is representative of a more aged plume 30 km
379 away, that may be physically and chemically evolved. The DOAS SO_2 column may thus be more
380 representative of the nearer source plume, however, our measurement in situ aerosol measurement
381 in the non-condensed plume (zone 2) will also depend on whether the balloon flight sampled the
382 more concentrated plume center or dilute plume edge. For comparison, Roberts et al. (2015) reports
383 $\sim 10^{15}$ particles of 0.20 – $100 \mu\text{m}$ size range per kg SO_2 at Mt Etna made by co-measured in-situ
384 aerosol and SO_2 .

385 The Holuhraun 2014-15 eruption emitted at least 3 times more SO_2 per day than the total of all
386 anthropogenic SO_2 sources across 28 European countries in 2010 (European Environmental Agency
387 (EEA), 2014). Fluxes of SO_2 have been reported of up to 120 kilotons per day (kt/d) in September
388 2014 (reducing to 20-60 kt/d between 6 and 22 September 2014), with an overall emission of $2.0 \pm$
389 0.6 Tg of SO_2 during the month of September and 11 ± 5 Tg of SO_2 for the whole active period
390 (Gíslason et al. 2015). We highlight that if our particle/ SO_2 ratio, $\sim 10^{13}$ – 10^{15} particles (0.2 - $100\mu\text{m}$

391 range) per kg SO₂ in the near-downwind plume estimated for 22 Jan 2015 is representative for the
392 volcanic source for the whole eruption period this yields a flux of up to ~10²²-10²⁴ particles per month
393 from Holuhraun, but further aerosol formation will occur by atmospheric oxidation of SO₂ as the
394 plume is dispersed and advected downwind, impacting both the free troposphere and ground-level
395 air quality at both local and regional scales (Schmidt et al., 2015). The particle surface area also plays
396 an important role in plume heterogeneous chemistry (Roberts et al., 2014), as well as climate
397 impacts (Schmidt et al., 2012).

398 5. Conclusion

399 This study demonstrated that the newly developed light balloon borne aerosol counter LOAC is an
400 effective method to detect and characterize a volcanic plume close to the crater. We have shown
401 that with this method, we were able to determine with a great accuracy the height of the top and the
402 bottom of the Holuhraun plume at a very specific location and time, and identify and characterize
403 distinct layers in the plume as a result of different hygroscopic phases of the plume based on the
404 observed aerosol size distribution.

405 Volcanic plumes are known to impact cloud formation and cloud properties through volcanic
406 sulfate aerosol that act as cloud condensation nuclei, (Martucci et al. 2012, Spiridonov et al. 2013).
407 However, for our observations the cloud rather likely formed due to the presence of hygroscopic
408 volcanic particles and excess water vapor in the near-source plume, noting volcanic emissions
409 commonly predominantly consist of H₂O with typically only <1 to 10 % sulfur compounds, typically
410 mostly as SO₂, e.g. Oppenheimer et al. (2011). For this near-source emission into a cold atmosphere,
411 the gaseous H₂O emission condenses onto the volcanic sulfate particles as the plume rises and cools
412 to lower temperature (resulting in higher RH). Such cloud formation may facilitate processes (e.g.
413 within cloud droplet SO₂ oxidation) that could alter the plume properties and downwind impacts.
414 Clouds are commonly observed on top of volcano summits, but their formation can simply be due to
415 orographic reasons, here the volcanic origins are evident.

416 We thereby demonstrate a new launch-on-command capacity for the combined volcano particle
417 and plume height characterization during major volcano eruption events that can be applied near to
418 source as shown in this study but also to the dispersed plume further downwind. Other flights
419 including a LOAC passing through volcanic plumes are under investigation. Meteorological balloons
420 with LOAC instrument payloads can be launched by non-specialist personnel and are low-cost
421 compared to other methods such as by aircraft, and can be operated under a wider range of volcano
422 hazard conditions. This method can potentially be used to sample the near-source volcano plume of
423 a large eruption that is being injected into the stratosphere. Several LOAC balloon payloads are being
424 kept ready for launch in Iceland and France as well as near volcanoes overseas (e.g. the island of la
425 Reunion) in preparation for future major eruption events.

426 Our observations of Holuhraun plume in an early “young plume” state provide a valuable in-situ
427 dataset for initialization of atmospheric models of the downwind plume dispersion to assess air
428 quality and climate impacts. Few such in-situ measurements exist but are essential because the
429 theoretical mechanisms dealing with plume dynamic and chemical processes are typically better
430 known than the detailed composition of the volcano plume both near the crater or far from the
431 source, as well as the actual injection altitudes of emissions which can vary in time during an
432 eruption with compositionally distinct plume at different altitudes. In future, we will also undertake
433 comparison of the data to measurements made far from the Holuhraun source, as well as inter-
434 compare the Holuhraun volcanic aerosol to that of other volcanoes measured using the LOAC either
435 by ground-based and balloon-based sampling, as well as remote sensing methods.

436 **Acknowledgments.**

437 The LOAC team of the LPC2E/CNRS warmly thank all the persons from Icelandic Meteorological Office
438 and the University of Reykjavik for their supports during this field campaign, especially Evgenia
439 Ilyinskaya and the Cambridge scientist teams who have accepted our presence in their field
440 campaign. Special many thanks to Haraldur Olafsson for his welcome on Iceland and his generosity.
441 Thanks to Richard Yeo and Njáll Fannar Reynisson for their remarkable professionalism and for the
442 ride.

443 We acknowledge the ECMWF Archive product and Metview platform for permit the calculus of the
444 backward trajectories. We also acknowledge the Icelandic team that produced the HARMONIE
445 outputs.

446 This work is supported by the LABEX VOLTAIRE (ANR-10-LABX-100-01) from University of Orléans.

447 EC and RGG were supported by the NERC Centre for Observation and Modelling of Earthquakes,
448 Volcanoes, and Tectonics (COMET) and from NERC grants NE/1015592/1 and NE/J023310/1.

450 **References:**

- 451 Arnalds, O.: Dust sources and deposition of aeolian materials in Iceland. *Icelandic Agricultural*
452 *Sciences* 23:3–21, 2010.
- 453 Bagnold, R. A.: *The Physics of Blown Sand and Desert Dunes*, Methuen, New York, 1941.
- 454 Baratoux, D., Mangold, N., Arnalds, O., Bardintzeff, J.M., Platevoet, B., Grégoire, M., Pinet, P.:
455 Volcanic sands of Iceland – Diverse origins of aeolian sand deposits revealed at Dyngjusandur and
456 Lambahraun. *Earth Surf. Proc. Land.* 36:1789-1808, 2011.
- 457 Barsotti, S., Neri, A., Scire, J. S.: The VOL-CALPUFF model for atmospheric ash dispersal: 1. Approach
458 and physical formulation, *J. Geophys. Res.*, 113, B03208, doi:10.1029/2006JB004623, 2008.
- 459 Brousseau, P., Berre, L., Bouttier, F., Desroziers, G.: Background-error covariances for a convective-
460 scale data-assimilation system: AROME–France 3D-Var. *Q. J. R. Meteorol. Soc.* 137: 409–422.
461 DOI:10.1002/qj.750, 2011.
- 462 Carboni, E., Grainger, R., Walker, J., Dudhia, A., Siddans, R.: A new scheme for sulphur dioxide
463 retrieval from IASI measurements: application to the Eyjafjallajökull eruption of April and May
464 2010, *Atmos. Chem. Phys.*, 12, 11417–11434, 2012/doi:10.5194/acp-12-11417-2012, 2012.
- 465 Carboni, E., Grainger, R. G., Mather, T. A., Pyle, D. M., Thomas, G., Siddans, R., Smith, A., Dudhia, A.,
466 Koukouli, M. L., and Balis, D.: The vertical distribution of volcanic SO₂ plumes measured by IASI,
467 *Atmos. Chem. Phys. Discuss.*, 15, 24643-24693, doi:10.5194/acpd-15-24643-2015, 2015.
- 468 Chuan, R. L., Palais, J., Rose, W. I., Kyle, P. R.: Fluxes, sizes, Morphology and compositions of particles
469 in the Mt. Erebus volcanic plume, December 1983, *Journal of Atmospheric Chemistry* 4 (1986), 467-
470 477, 1986.
- 471 Dagsson-Waldhauserova, P., Arnalds, O., Olafsson, H.: Long-term frequency and characteristics of
472 dust storm events in Northeast Iceland (1949-2011). *Atmospheric Environment* 77, 117-127, 2013.
- 473 Dagsson-Waldhauserova, P., Arnalds, O., Olafsson, H.: Long-term variability of dust events in Iceland.
474 *Atmospheric Chemistry and Physics* 14, 13411-13422. DOI:10.5194/acp-14-13411-2014, 2014.
- 475 Deshler, T., Hervig, M. E., Hofmann, D. J., Rosen, J. M., Liley, J. B.: Thirty years of in situ stratospheric
476 aerosol size distribution measurements from Laramie, Wyoming (41N), using balloon-borne
477 instruments, *J. Geophys. Res.*, 108(D5), 4167, doi:10.1029/2002JD002514, 2003.
- 478 Galle, B., Johansson, M., Rivera, C., Zhang Y., Kihlman, M., Kern, C., Lehmann T., Platt, U., Arellano, S.,
479 and S. Hidalgo (2010), Network for Observation of Volcanic and Atmospheric Change (NOVAC)—A
480 global network for volcanic gas monitoring: Network layout and instrument description, *J. Geophys.*
481 *Res.*, 115, D05304, doi:10.1029/2009JD011823
- 482 Gíslason, S.R., Stefánsdóttir, G., Pfeffer, M.A., Barsotti, S., Jóhannsson, Th., Galeczka, I., Bali, E.,
483 Sigmarsson, O., Stefánsson, A., Keller, N.S., Sigurdsson, Á., Bergsson, B., Galle, B., Jacobo, V.C.,
484 Arellano, S., Aiuppa, A., Jónasdóttir, E.B., Eiríksdóttir, E.S., Jakobsson, S., Guðfinnsson, G.H.,
485 alldórsson, S.A., Gunnarsson, H., Haddadi, B., Jónsdóttir, I., Thordarson, Th., Riishuus, M.,
486 ögnadóttir, Th., Dürig, T., Pedersen, G.B.M., Höskuldsson, Á., Gudmundsson, M.T.: Environmental
487 pressure from the 2014–15 eruption of Bárðarbunga volcano, Iceland. *Geochem. Persp. Let.* 1, 84-
488 93, 2015.

489 Hammer, E., Gysel, M., Roberts, G. C., Elias, T., Hofer, J., Hoyle, C. R., Bukowiecki, N., Dupont, J.-C.,
490 Burnet, F., Baltensperger, U., Weingartner, E.: Size-dependent particle activation properties in fog
491 during the ParisFog 2012/13 field campaign, *Atmos. Chem. Phys.*, 2014/05/15 6.81, 2014.

492 Ialongo, I., Hakkarainen, J., Kivi, R., Anttila, P., Krotkov, N.A.N., Yang, K., Li, C., Tukiainen, S., Hassinen,
493 S., Tamminen, J.: Comparison of operational satellite SO₂ products with ground-based observations
494 in northern Finland during the Icelandic Holuhraun fissure eruption, *Atmos. Meas. Tech.* 2015, Vol.
495 8 Issue 6, p2279-2289. 11p. DOI:10.5194/amt-8-2279-2015, 2015.

496 Junge, C.E., Chagnon, C.W., Manson, J.E.: STRATOSPHERIC AEROSOLS. *J. Meteor.*, 18, 81–108. doi:
497 [http://dx.doi.org/10.1175/1520-0469\(1961\)018<0081:SA>2.0.CO;2](http://dx.doi.org/10.1175/1520-0469(1961)018<0081:SA>2.0.CO;2), 1961.

498 Kroll, J.H., Cross, E.S., Hunter, J.F, Pai, S., Wallace, L.M.M., Croteau, P.L., Jayne, J.T., Worsnop, D.R.,
499 Heald, C.L., Murphy, J.G., Frankel, S.L.: Atmospheric Evolution of Sulfur Emissions from Kīlauea:
500 Real-Time Measurements of Oxidation, Dilution, and Neutralization within a Volcanic Plume.
501 *Environmental science & technology* 49, no. 7: 4129-4137, 2015.

502 Martucci, G., Ovadnevaite, J., Ceburnis, D., Berresheim, S., Varghese, S., Martin, D., Flanagan, R.,
503 O’Dowd, C.D.: Impact of volcanic ash plume aerosol on cloud microphysics, *Atmos. Env.* 48 205-218,
504 2012.

505 McGonigle, A. J. S., Aiuppa, A., Giudice, G., Tamburello, G., Hodson, A. J., and Gurrieri, S.: Unmanned
506 aerial vehicle measurements of volcanic carbon dioxide fluxes, *Geophys. Res. Lett.*, 35, L06303,
507 doi:10.1029/2007GL032508; 2008.

508 Óladóttir, B., Larsen, G., Sigmarsson, O. : Holocene volcanic activity at Grímsvötn, Bárðarbunga and
509 Kverkfjöll subglacial centres beneath Vatnajökull, Iceland. *Bulletin of Volcanology* 73,1187-1208,
510 2011.

511 Óladóttir, B.A., Sigmarsson, O., Larsen, G., Devidal, J.L. : Provenance of basaltic tephra from
512 Vatnajökull subglacial volcanoes, Iceland, as determined by major- and trace-element analyses. *The*
513 *Holocene* 21:1037–1048, 2011.

514 Oppenheimer C., Scaillet B., and Martin R. S.: Sulfur degassing from volcanoes: source conditions,
515 surveillance, plume chemistry and earth system impacts." *Reviews in mineralogy and geochemistry*
516 73, no. 1, 363-421, 2011.

517 Pieri, D., Diaz, J.A., Bland, G., Fladeland, M., Madrigal, Y., Corrales, E., Alegria, O., et al. : In situ
518 observations and sampling of volcanic emissions with NASA and UCR unmanned aircraft, including a
519 case study at Turrialba Volcano, Costa Rica." *Geological Society, London, Special Publications* 380,
520 no. 1: 321-352, 2013.

521 Renard, J.B., Berthet, G., Salazar, V., Catoire, V., Tagger, M., Gaubicher, B., Robert, C.: In situ
522 detection of aerosol layers in the middle stratosphere, *Geophys. Res. Lett.*, 37, L20803,
523 doi:10.1029/2010GL044307, 2010.

524 Renard, J.B., Dulac, F., Berthet, G., Lurton, T., Vignelles, D., Jégou, F., Tonnelier, T., Thauray, C.,
525 Jeannot, M., Couté, B., Akiki, R., Verdier, N., Mallet, M., Gensdarmes, F., Charpentier, P., Duverger,
526 V., Dupont, J.V., Mesmin, S., Elias, T., Crenn, V., Sciare, J., Giacomoni, J., Gobbi, M., Hamonou, E.,
527 Ólafsson, H., Dagsson-Waldhauserova, P., Camy-Peyret, C., Mazel, C., Décamps, T., Piringer, M.,
528 Surcin, J., and Daugeron, D.: LOAC: a small aerosol optical counter/sizer for ground-based and
529 balloon measurements of the size distribution and nature of atmospheric particles – Part 1:

530 Principle of measurements and instrument evaluation, *Atmos. Meas. Tech. Discuss.*, 8, 9993-10056,
531 doi:10.5194/amtd-8-9993-2015, 2015.

532 Rodgers, C.D.: *Inverse Methods for Atmospheric Sounding: Theory and Practice*, World Scientific
533 Publishing Co. Ltd., 2000.

534 Roberts, T.J., Martin, R.S., Jourdain L.: Reactive bromine chemistry in Mount Etna's volcanic plume:
535 the influence of total Br, high-temperature processing, aerosol loading and plume–air mixing,
536 *Atmospheric Chemistry and Physics*, 14, 20, 11201-11219, 2014.

537 Roberts T.J., Vignelles D., Liuzzo M., Giudice G., Aiuppa A., Chartier M., Coute B., Lurton T., Berthet
538 G., Renard J.-B.: Advances in in-situ real-time monitoring of volcanic emissions: HCl, and size-
539 resolved aerosol at Mt Etna (passive degassing), submitted to *Geochimica et Cosmochimica Acta*,
540 2015.

541 Saunders, R. W., Matricardi, M., and Brunel, P.: An improved fast radiative transfer model for
542 assimilation of satellite radiance observations, *Q. J. Roy. Meteor. Soc.*, 125, 1407–1425,
543 doi:10.1002/qj.1999.49712555615 , 1999.

544 Shinohara, H.: Composition of volcanic gases emitted during repeating Vulcanian eruption stage of
545 Shinmoedake, Kirishima volcano, Japan. *Earth, Planets and Space*, 65, 6: 667-675, 2013.

546 Schmidt, A., Leadbetter, S., Theys, N., Carboni, E., Withman, C.S., Stevenson, J.A., Birch, C.E.,
547 Thordarson, T., Turnock, S., Barsotti, S., Delaney, L., Feng, W., Grainger, R.G., Hort, M.C.,
548 Höskuldsson, À., Ialongo, I., Ilyinskaya, E., Jóhannsson, T., Kenny, P., Mather, T.A., Richards, N.A.D.,
549 Sheperd, J.: Satellite detection, long-range transport, and air quality impacts of volcanic sulfur
550 dioxide from the 2014–2015 flood lava eruption at Bárðarbunga (Iceland), *J. Geophys. Res. Atmos.*,
551 120, doi:10.1002/ 2015JD02363, 2015.

552 Schmidt, A., Ostro, B., Carslaw, K.S., Wilson, M., Thordarson, Th., Mann, G.W., Simmons A.J.: Excess
553 Mortality in Europe Following a Future Laki-Style Icelandic Eruption. *Proceedings of the National*
554 *Academy of Sciences* 108, no. 38: 15710–15. doi:10.1073/pnas.1108569108, 2011.

555 Spinetti, C., Barsotti, S., Neri, A., Buongiorno, M.F., Doumaz, F., Nannipieri, L.: Investigation of the
556 complex dynamics and structure of the 2010 Eyjafjallajökull volcanic ash cloud using multispectral
557 images and numerical simulations, *J. Geophys. Res. Atmos.*, 118, 4729–4747,
558 doi:10.1002/jgrd.50328, 2013.

559 Y. Seity, Brousseau, P., Malardel, S., Hello, G., Bénard, P., Bouttier, F., Lac, C., Masson, V.: The
560 AROME-France Convective-Scale Operational Model. *Mon. Wea. Rev.*, 139, 976–991,
561 2011. Spiridonov, V. and Curic, M.: Evaluation of the physical and chemical properties of
562 Eyjafjallajökull volcanic plume using a cloud-resolving model. *Pure and applied Geophysics*. 170
563 (2013) 1729-1750, 2013.

564 Thordarson, T., and Self, S.: Atmospheric and Environmental Effects of the 1783–1784 Laki Eruption:
565 A Review and Reassessment. *J. Geophys. Res.* 108, no. D1 (January 8, 2003): 4011., 2003.

566 Van Eaton, A. R., Herzog, M., Wilson, C.J.N., McGregor, J.: Ascent dynamics of large phreatomagmatic
567 eruption clouds: The role of microphysics, *J. Geophys. Res.*, 117, B03203,
568 doi:10.1029/2011JB008892, 2012.

569 Vernier, J.-P., et al., Major influence of tropical volcanic eruptions on the stratospheric aerosol layer
570 during the last decade, *Geophys. Res. Lett.*, 38, L12807, doi:10.1029/2011GL047563, 2011.

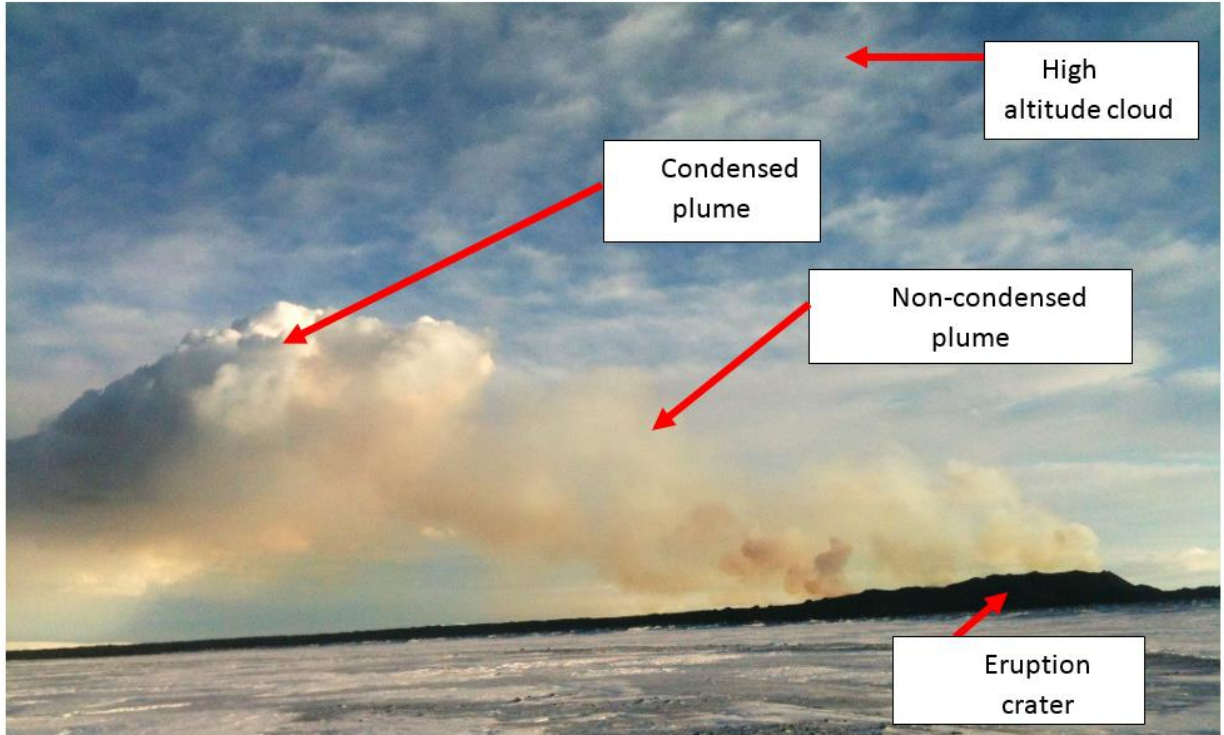
- 571 Warner, J.: The Microstructure of Cumulus Cloud. Part I. General Features of the Droplet Spectrum. J.
572 Atmos. Sci., 26, 1049–1059. doi: <http://dx.doi.org/10.1175/1520->
573 [0469\(1969\)026<1049:TMOCCP>2.0.CO;2](http://dx.doi.org/10.1175/1520-0469(1969)026<1049:TMOCCP>2.0.CO;2), 1969.
- 574 Warner, J.: The Microstructure of Cumulus Cloud. Part II. The Effect on Droplet Size Distribution of
575 the Cloud Nucleus Spectrum and Updraft Velocity. J. Atmos. Sci., 26, 1272–1282. doi:
576 [http://dx.doi.org/10.1175/1520-0469\(1969\)026<1272:TMOCCP>2.0.CO;2](http://dx.doi.org/10.1175/1520-0469(1969)026<1272:TMOCCP>2.0.CO;2), 1969.
- 577 Witham, C. S., Oppenheimer, C.: Mortality in England during the 1783–4 Laki Craters Eruption.
578 Bulletin of Volcanology 67, no. 1 (May 11, 2004): 15–26. doi:[10.1007/s00445-004-0357-7](https://doi.org/10.1007/s00445-004-0357-7), 2004.
- 579

580
$$V(d) = \frac{V_0}{\sigma_N \sqrt{2\pi}} e^{\left(-\frac{1}{2} \left(\frac{\log(d) - \mu_v}{\sigma_N}\right)^2\right)} \quad (1)$$

581 Where $V(d)$ is the volume density distribution with shape parameters: σ_N and μ_v and the
582 amplitude parameter V_0 .

583 **Equation 1.** Calculated density distribution for the volume from shape parameters giving by less-
584 square fitting

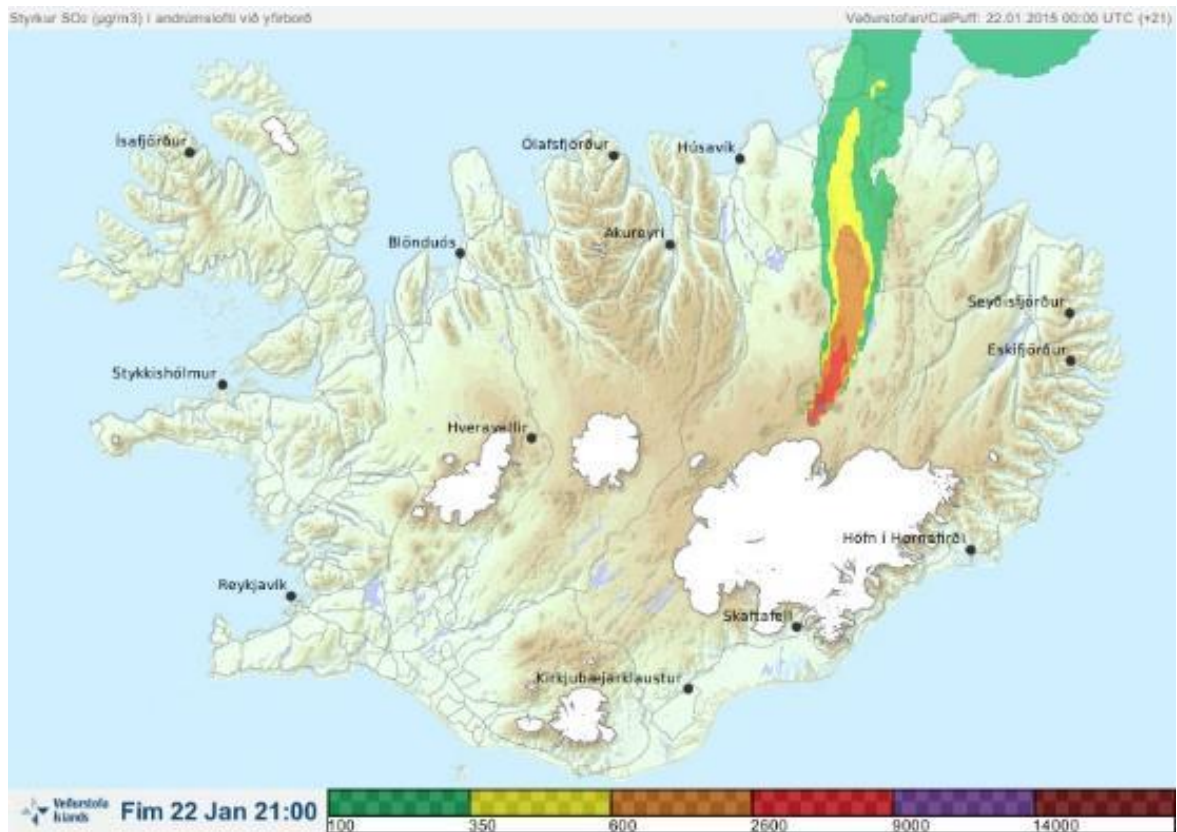
585



586

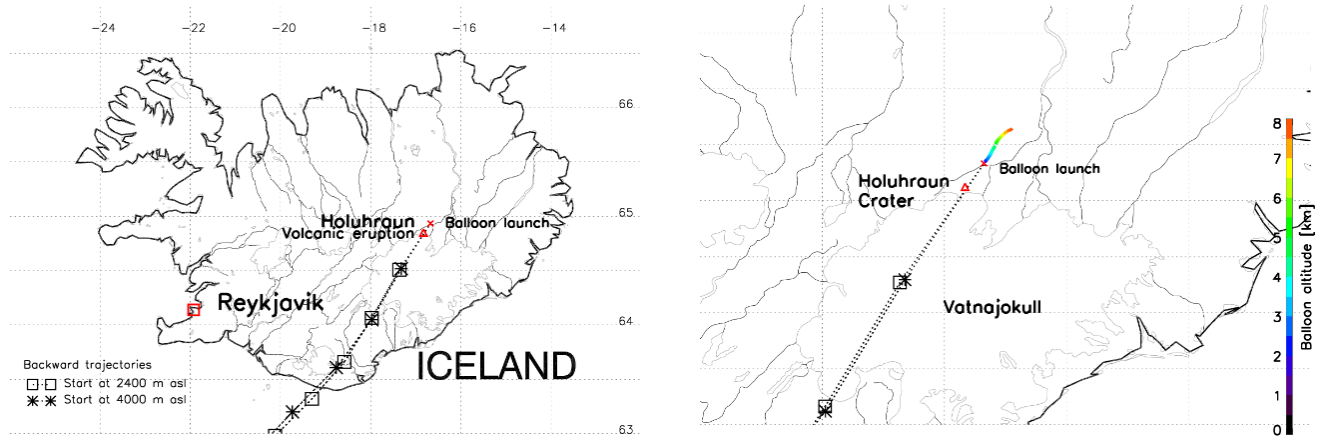
587

Figure 1. Picture taken at 14UTC on January 22nd during the afternoon before the balloon flight.



588
 589
 590
 591
 592
 593
 594

Figure 2. Forecast from the Icelandic Meteorological Office showing the direction of the plume and the concentration in $\mu\text{g}/\text{m}^3$ of SO_2 at 22UTC on the January 22th, less than 30 minutes before the balloon launch. This forecast was used on the campaign field in order to take the decision to launch the balloon. During the daytime the plume direction was going to the East, which didn't represented a good solution for make the balloon borne profile near to the crater.



595

596

597

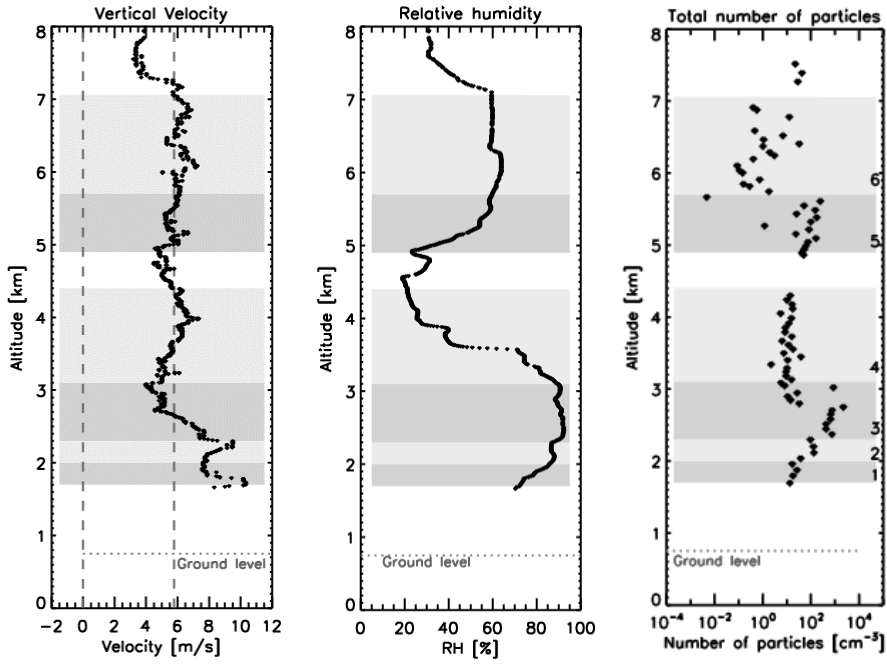
598

599

600

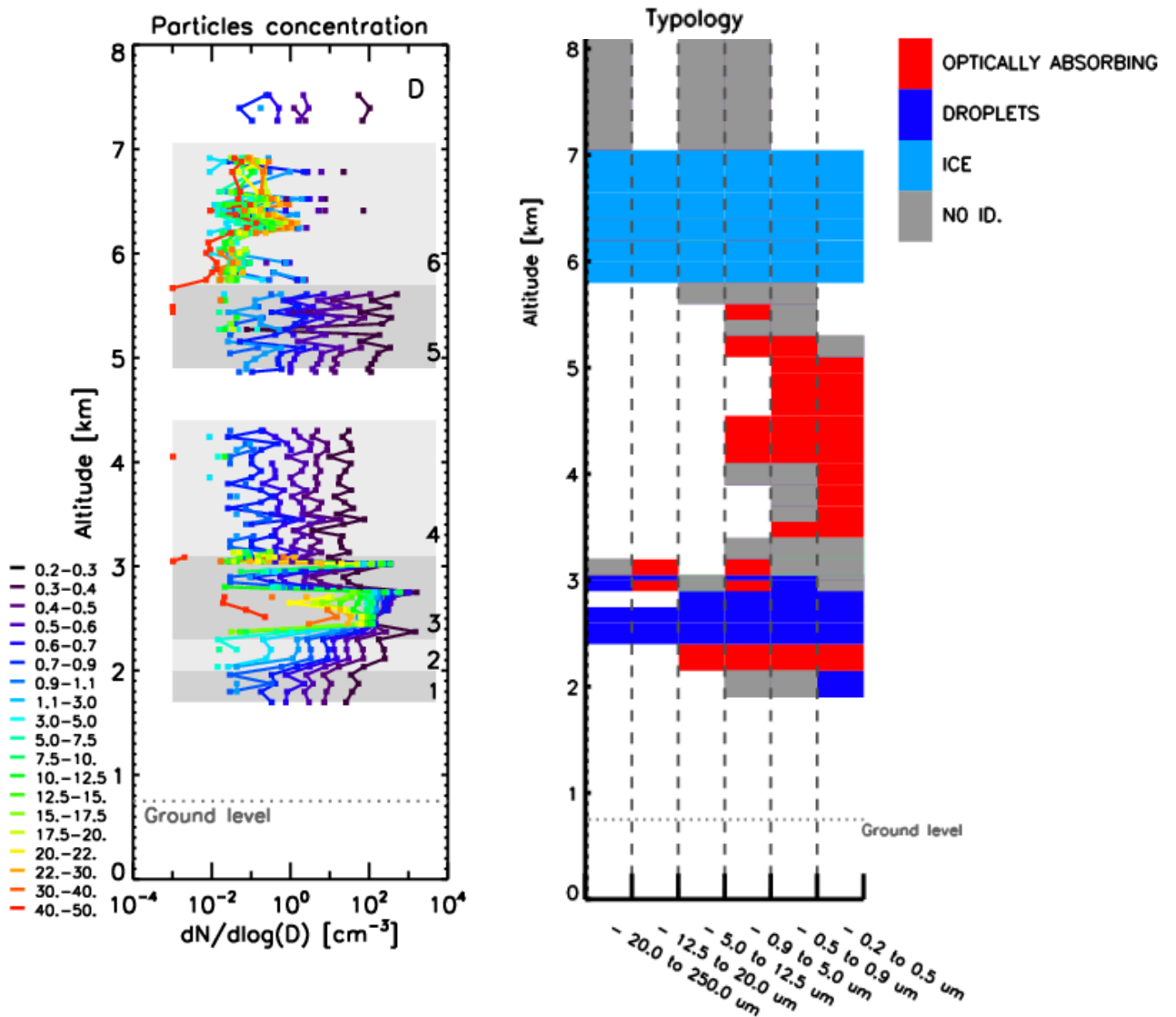
601

Figure 3. Localization of the launch, on the left: general view, the Holuhraun eruption is located by a red triangle and the balloon launch by a red cross. On the right: focus on the Holuhraun crater, the balloon flight path is represented as a function of altitude referred by the key on the right. For both panels, we add two time backward trajectories intersecting the balloon launch position at 2400 m and 4000m. These trajectories are calculated using FLEXTRA code initialized with ECMWF wind fields of January 22nd at 21UTC above the balloon launch position.

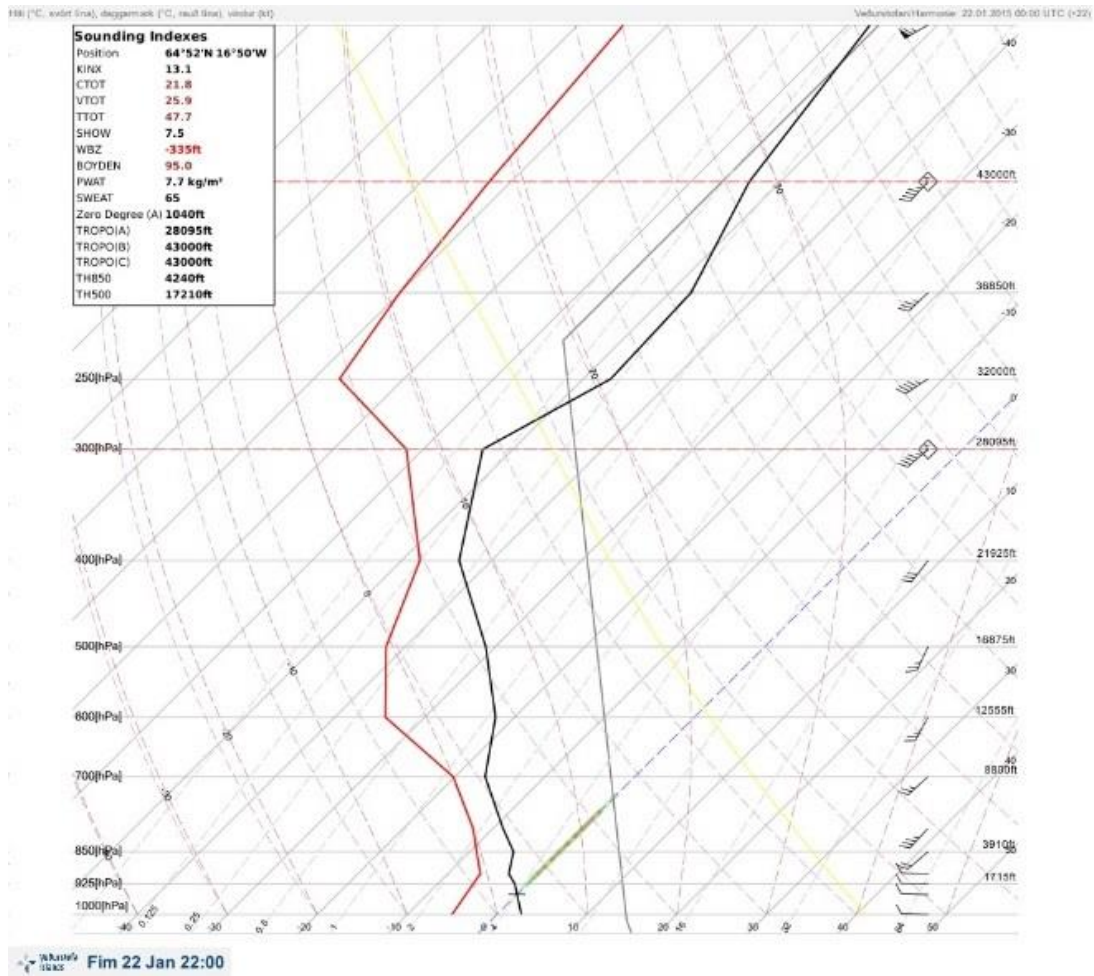


602 **Figure 4.** Flight parameters measured during the balloon ascent. A: Vertical velocity, B: Relative
 603 humidity, C: Total particles concentration (from 0.2 to 100 μm).

604



605 **Figure 5.** On the left: Normalized concentration of aerosols for each size class as a function of
606 altitude. Each color is relative to a size class, the key is on the left. On the right and for the same
607 altitudes, Typology : main optical nature for 6 super-size classes as a function of altitude.
608



610

611 **Figure 6.** Outputs from the HARMONIE model for the Holuhraun region (64°52'N and 16°50'W)
 612 over a 2.5 km square region, showing the column profile over the fissural eruption at 22UTC, time of
 613 the balloon launch. The red line represents the dew point and the black line the temperature
 614 simulated. When the temperature and the dew point match the air is saturated and we expect a
 615 cloud. Here, the model does not predict any cloud.

616

617

618
619
620
621
622
623

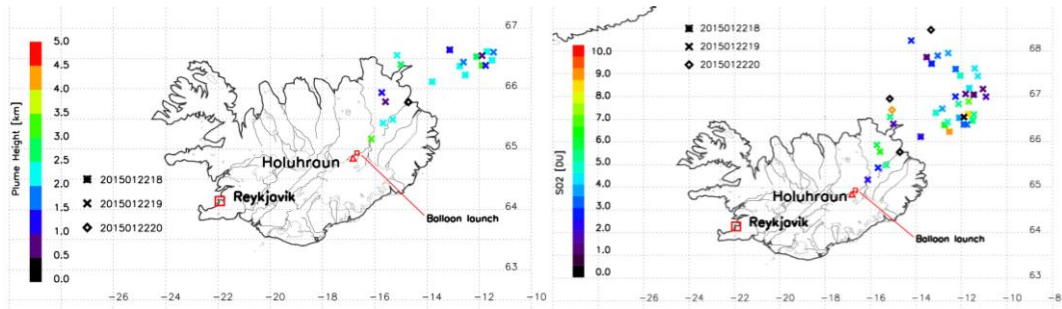
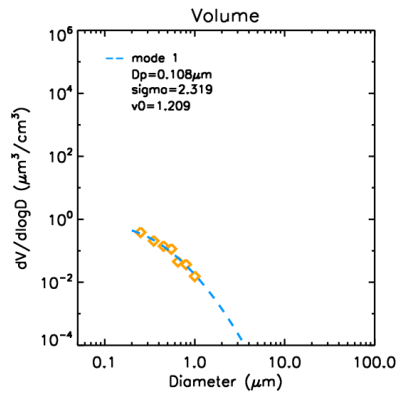
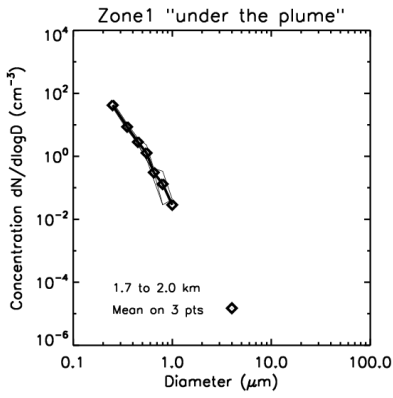
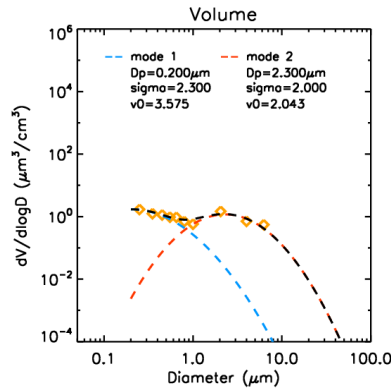
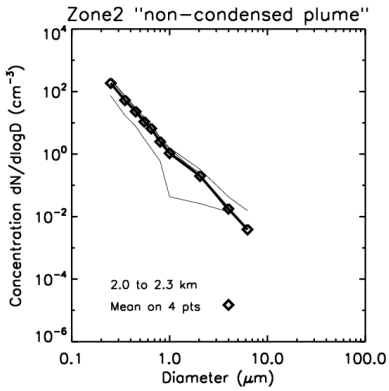


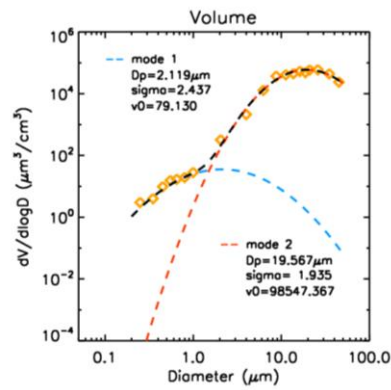
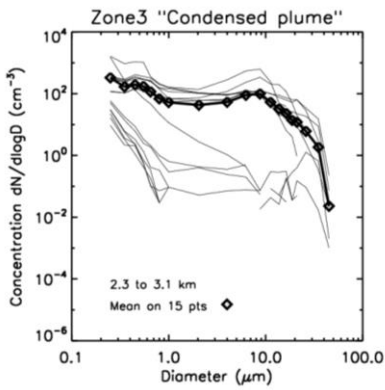
Figure 7. Left: height of the plume for three overpasses at 18, 19 and 20UTC on January 22th from IASI retrieval method in Carboni et al. 2012. Right: SO₂ in Dobson units for the same three overpasses.



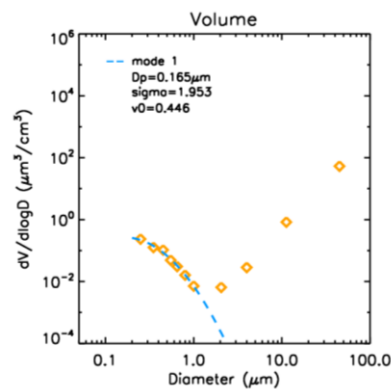
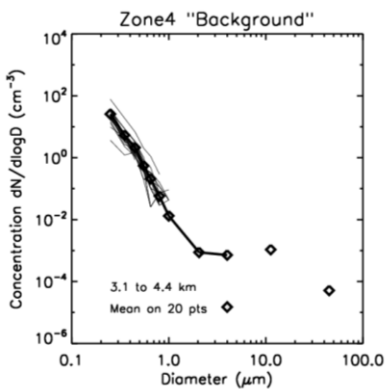
624



625



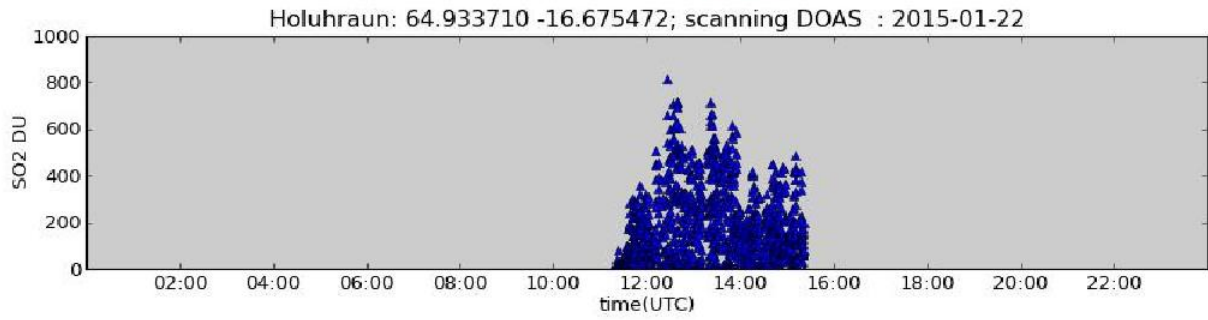
626



627

628

Figure 8: Size-distribution by number and by volume with lognormal fit for the zone 1 to 4.



629

630

631

632

Figure 9. Time series on January 22nd 2015 of the column density of SO₂ detected by NOVAC scanning DOAS positioned 10 km from the eruption site. An average emission rate of 400 kg/s SO₂ for this day is calculated.

	Zone 1	Zone 2		Zone 3		Zone 4
	From 1.7 to 2.0 km	From 2.0 to 2.3 km		From 2.3 to 3.1 km		From 3.1 to 4.4 km
	<i>Under the plume</i>	<i>Non-condensed plume</i>		<i>Condensed plume</i>		<i>Background</i>
		Mode 1	Mode 2	Mode 1	Mode 2	
Mean diameter [μm]	0.1	0.2	2.3	2.1	19.6	0.1
Standard deviation [μm]	2.3	2.3	2.0	2.4	1.9	2.0
Total volume [μm³]	1.2	3.6	2.0	79.1	98547.3	0.4

633

634 Table 1: Parameters from the log-normal fitting on volumic concentration measured by LOAC for
635 the first four zones determined. Zone 1 and zone 4 are assumed as the “clean” air mass in which the
636 plume is advected and measured in zone 2 and 3.

637